JACS
JOURNAL OF THE AMERICAN CHEMICAL SOCIETY

Communication

pubs.acs.org/JACS

Resonant Charge Transport in Conjugated Molecular Wires beyond 10 nm Range

Guowen Kuang,[†] Shi-Zhang Chen,[‡] Weihua Wang,[†] Tao Lin,[†] Keqiu Chen,[‡] Xuesong Shang,[§] Pei Nian Liu,*[,§] and Nian Lin*[,†]

[†]Department of Physics, The Hong Kong University of Science and Technology, Hong Kong, China

[‡]Department of Applied Physics, School of Physics and Electronics, Hunan University, Changsha 410082, China

[§]Shanghai Key Laboratory of Functional Materials Chemistry and Institute of Fine Chemicals, East China University of Science and Technology, Meilong Road 130, Shanghai 200237, China

Supporting Information

ABSTRACT: Using a scanning tunneling microscope, we measured high-bias conductance of single polyporphyrin molecular wires with lengths from 1.3 to 13 nm. We observed several remarkable transport characteristics, including multiple sharp conductance peaks, conductances as high as 20 nS in wires with lengths of >10 nm, and nearly length-independent conductance (attenuation <0.001 $Å^{-1}$). We carried out first-principles simulations on myriad metal−molecule−metal junctions. The simulations revealed that the measured conductance is coherent resonant transport via a delocalized molecular orbital.

Efficient long-range charge transport in molecular wires is of great importance in molecular electronic devices such as light-emitting diodes, field-effect transistors, spintronics, and solar cells, to name a few.[1] Charge transport over a long range is expected to be conceptually different from that in short molecules (<3 nm), wherein off-resonant tunneling dominates the charge transport and decays exponentially.[2] In the longer regime (>6 nm), incoherent sequential hopping is widely accepted as the major charge transport mechanism, whose conductance features a power law decay.[3] A more effective long-range charge transport mechanism is resonant transport. Resonant transport, which takes place when a frontier molecular orbital aligns with the Fermi level of the electrodes,[4] can be nearly length-independent.[5] Long-range resonant transport was reported in nanotubes and DNA wires.[6]

Porphyrin-based molecular wires can mediate charge transport with attenuation factors below 0.1 $Å^{-1}$.[7−11] Charge transport in these systems occurs via off-resonant tunneling in short wires and hole polaron delocalization in long wires.[8−11] In this work, we studied charge transport through biphenyl−porphyrin oligomer (***bp-ppo***) wires with lengths of 1.3 to 13 nm. The ***bp-ppo*** wires were synthesized using on-surface Ullmann reaction from precursor molecules of 5,15-bis(4-bromophenyl)-10,20-diphenylporphyrin (Br_2-TPP) (Figure 1a) on a Au(111) surface.[12] Figure 1b shows the ***bp-ppo*** wires comprising different numbers of TPP units. We applied on-surface metalation to convert free-base ***bp-ppo*** wires to Fe-***bp-ppo*** wires.[13a,b]

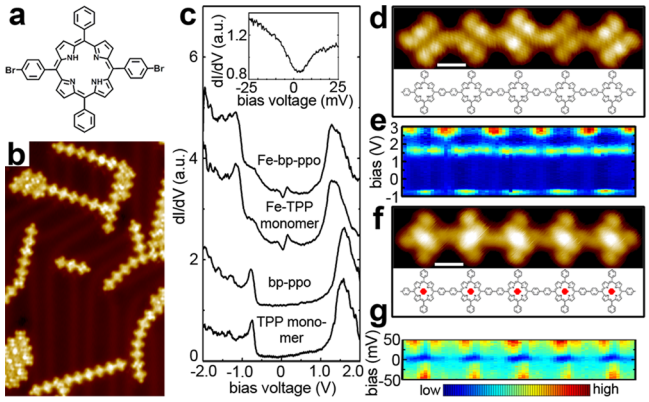

Figure 1. (a) Precursor Br_2-TPP molecule. (b) STM topograph (40 nm × 25 nm) showing ***bp-ppo*** wires synthesized on a Au(111) surface. (c) From bottom to top: tunneling spectra of a Br_2-TPP monomer, a TPP unit in a ***bp-ppo*** wire, an Fe-TPP monomer, and an Fe-TPP unit in an Fe-***bp-ppo*** wire. Inset: zero-bias dip in the Fe-TPP tunneling spectrum. (d, f) STM topographs of (d) a five-unit ***bp-ppo*** wire and (f) a five-unit Fe-***bp-ppo*** wire, with corresponding chemical structures. (e, g) Spatially resolved dI/dV maps of (e) the ***bp-ppo*** wire and (g) the Fe-***bp-ppo*** wire. All scale bars are 1 nm.

Figure 1c shows, from bottom to top, representative differential tunneling spectra measured at the center of a Br_2-TPP monomer, a TPP unit in a ***bp-ppo*** wire, an Fe-TPP monomer, and an Fe-TPP unit in an Fe-***bp-ppo*** wire. The units in the wires display nearly identical characteristics as the corresponding monomers, implying that the biphenyl linkers do not shift the frontier molecular orbitals of the porphyrin units in the wires. TPP features two peaks at 1.6 and −0.9 V. Density functional theory calculations confirmed that the 1.6 V peak is associated with the lowest unoccupied molecular orbital (LUMO) and LUMO+1 and that the −0.9 V peak is associated with the highest occupied molecular orbital (HOMO).[13c] Fe-TPP also features two peaks, which are downshifted to 1.4 and −1.2 V. The major difference between TPP and Fe-TPP is that Fe-TPP has a zero-bias dip and a low-energy peak at 0.2 V. The zero-bias conductance dip (Figure 1c inset) manifests Kondo resonance associated with Fe spin states.[13b] Figure 1d is a high-

Received: July 21, 2016
Published: August 23, 2016

DOI: 10.1021/jacs.6b07416
J. Am. Chem. Soc. 2016, 138, 11140−11143

resolution scanning tunneling microscopy (STM) image of a five-unit ***bp-ppo*** wire and its chemical structure. Spatially resolved point-by-point dI/dV spectra along the central axis of this wire (Figure 1e) reveal that the HOMO is distributed primarily at the porphyrin moieties, whereas the LUMO/LUMO+1 is delocalized along the wire backbone. Figure 1f shows a five-unit Fe-***bp-ppo*** wire in which the central protrusions of the TPP units account for Fe. The Fe sites show a reduced dI/dV signal at the Fermi level (Figure 1g) as a result of the Kondo effect. With a wide bias window, the spatially resolved dI/dV map of the Fe-***bp-ppo*** wire displays features very similar to those of the ***bp-ppo*** wire shown in Figure 1e, indicating that the Fe centers do not affect the frontier molecular orbitals.

We used the STM tip to lift the wires as illustrated in Figure 2a.[14,15] Figure 2b–d shows a seven-unit ***bp-ppo*** wire that was

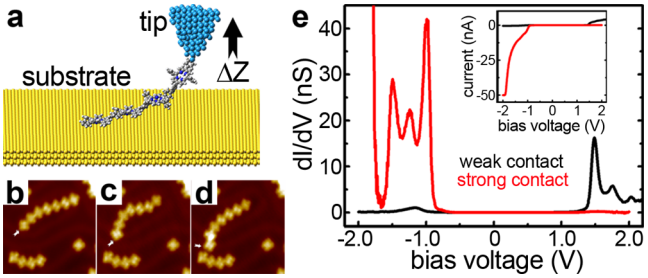

Figure 2. (a) Schematic illustration of short-range transport. (b–d) STM topographs showing repeated lifting and dropping of a seven-unit ***bp-ppo*** wire. Arrows mark the contact points of individual manipulations. (e) dI/dV vs V curves measured at a tip height of 1.3 nm with weak contact (black) and strong contact (red). Inset: I–V plot.

repeatedly lifted and dropped; the contact point of each manipulation is marked with an arrow. In the first two manipulations, the contact was lost and the wire dropped when the tip was retracted 2 nm from the set point. In the third manipulation, the tip was retracted to 8 nm without losing the contact, presumably sustained by a stronger tip–molecule contact than in the first two manipulations. Such weak and strong contacts were highly reproducible in our experiments. We propose that the strong contact corresponds to covalent bonding between the terminal TPP units and the apex atom of the STM tip, while the weak contact corresponds to physisorption of the terminal TPP to the tip.

Figure 2e presents two differential conductance curves measured at a tip retraction of 1.3 nm in the weak contact (black) and strong contact (red) configurations. The initial tip height was about 0.7 nm above the substrate; thus, at a tip retraction of 1.3 nm, the tip apex was ∼2.0 nm above the substrate, and thus approximately one TPP unit was bridged between the tip and the substrate. We define the transport measured at this tip height as short-range transport. With weak contact, a salient peak of 15 nS appeared at 1.5 V, accompanied by two satellite peaks at 1.75 and 2.0 V, and a weak peak of 1 nS appeared at −1.2 V. With strong contact, three peaks of 40, 22, and 28 nS appeared at −1.0, −1.2, and −1.4 V, respectively.

We performed first-principles calculations to simulate the short-range transport. A single TPP molecule bridges a flat Au substrate and a pyramid-shaped tip (Figure 3a) to form a metal–molecule–metal junction. Two configurations were considered: with the top phenyl moiety physically attached to

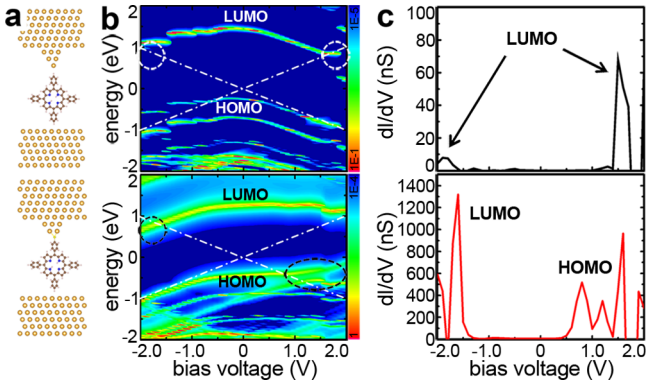

Figure 3. (a) Simulated junctions of a single TPP coupled to the tip weakly (top) or strongly (bottom). (b) Simulated transmission as a function of tip–substrate bias and energy for the two models. (c) Simulated dI/dV vs V traces for the two junctions.

the tip, simulating weak contact (Figure 3a, top), and with the top phenyl moiety covalently bonded to the tip via a Au–S bond, simulating strong contact (Figure 3a, bottom). In both models, the bottom phenyl moieties are weakly coupled to the substrate. Figure 3b shows the calculated transmission as a function of tip–substrate bias and energy. The areas inside the dashed crosses refer to the conductance window; transmission signals inside this region contribute to conductance. With weak contact (Figure 3b, top), the LUMO enters the conductance window at 1.5 and −1.8 V (marked by the white circles). As a result, the differential conductance (Figure 3c, top) features a 70 nS conductance peak at 1.5 V and a 10 nS peak at −1.8 V. In comparison, the HOMO contribution is insignificant. With strong contact (Figure 3b, bottom), the LUMO enters the conductance window at −1.8 V (black circle at the left), resulting in a 1300 nS conductance peak at −1.8 V (Figure 3c, bottom). At positive bias, HOMO, HOMO−1 and HOMO−2 enter the conductance window at positive bias (black circle at the right), contributing three conductance peaks at 0.8, 1.2, and 1.5 V (Figure 3c, bottom). The LUMO-channeled conductance peaks of the two junctions are in good agreement with the experimental data shown in Figure 2e. However, the positive-bias peaks channeled by the HOMO in the strong contact junction are not present in the experimental data. We suggest that this discrepancy is caused by inaccurate HOMO energy level obtained in the simulation (see the SI for details). The multiple satellite peaks resolved in the experiments are presumably associated with molecular vibrational modes,[16,17] which were ignored in our calculations.

Wires with strong contact can be lifted entirely off the substrate. The largest tip retraction with the wire bridging the tip and the substrate was 13 nm, corresponding to at least eight TPP units hanging between the tip and the surface, as illustrated in Figure 4a. We define the conductance measured in this configuration as long-range transport. We measured the long-range transport of dozens of ***bp-ppo*** wires and Fe-***bp-ppo*** wires and found no systematic distinction between the conductance characteristics of the two, suggesting that the conductance is mediated by the molecular backbones but not the Fe centers. This behavior is in contrast to the low-bias transport of porphyrin molecules, in which a metal center enhances the conductance.[18] Figure 4b,c shows five differential conductance curves acquired at the indicated tip retraction heights of a five-unit ***bp-ppo*** wire and a 10-unit Fe-***bp-ppo*** wire

DOI: 10.1021/jacs.6b07416
J. Am. Chem. Soc. 2016, 138, 11140–11143

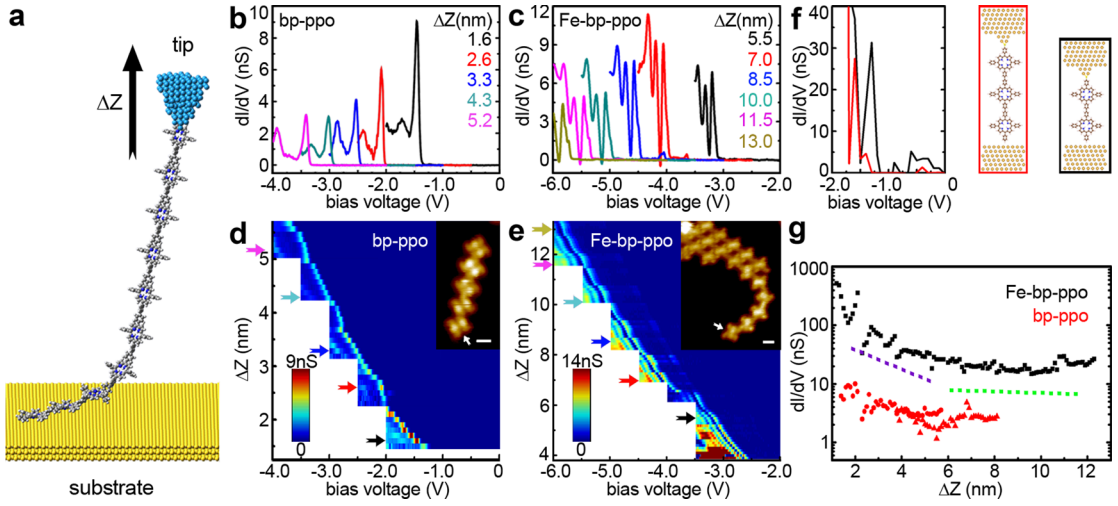

Figure 4. (a) Schematic illustration of long-range transport. (b, c) dI/dV vs V traces of a ***bp-ppo*** wire (shown in the inset in (d)) and a Fe-***bp-ppo*** wire (shown in the inset in (e)) acquired at the tip retraction heights indicated by the arrows in (d) and (e). (d, e) Length-dependent differential conductance maps acquired on (d) the ***bp-ppo*** wire and (e) the Fe-***bp-ppo*** wire. Scale bars in the insets are 1 nm. (f) Calculated dI/dV vs V traces of a double-unit ***bp-ppo*** junction (black) and a triple-unit ***bp-ppo*** junction (red) as illustrated in the models. (g) Differential conductance of the ***bp-ppo*** wire and the Fe-***bp-ppo*** wire plotted against tip retraction height.

(insets in Figure 4d,e), respectively. One can see that multiple sharp conductance peaks are present at all tip retraction heights. The conductance peaks shift to more negative bias with increasing wire length. The series of dI/dV versus V curves acquired at progressively increased tip retraction heights were combined into maps displaying differential conductance (color scale) against tip height (y axis) and bias voltage (x axis) (Figure 4d,e). Since the tip retraction height defines the length of wire that bridges the tip and the substrate, such maps represent length-dependent differential conductance (LDC). The LDC maps show that the shifting rate of the conductance peaks is ∼0.3 V/nm and that the shifting is not perfectly linear but rather exhibits discontinuity with a periodicity of ∼1.2 nm. This behavior is attributed to lifting of successive TPP units from the substrate.[14a] One possible mechanism for the observed shift in the conductance peaks as a function of wire length is that the bias voltage is partitioned at the wire and the contacts in the metal−molecule−metal junctions as a function of wire length (see the SI for details).

Figure 4g shows plots of the values of the first conductance peaks shown in Figure 4d,e against tip retraction height. Despite the different magnitudes, the two wires exhibit very similar decay characteristics in their conductance. The conductance jumps at some tip heights.[14a] In spite of these irregularities, a trend of decay in the conductance as a function of wire length can be determined, as represented by the dotted lines in Figure 4g. When the tip retraction is <5 nm, the conductance decays with an attenuation factor of 0.04 Å^{-1} (purple dotted line). When the tip is retracted >6 nm, the conductance fluctuates around 20 nS (Fe-***bp-ppo***) or 3 nS (***bp-ppo***) until the wire is fully lifted from the substrate. For reference, we have plotted an exponential decay with an attenuation factor of 0.001 Å^{-1} (green dotted line in Figure 4g). This value is the lowest among all previously reported attenuation factors.[3f] Furthermore, Figure 4g shows that the experimental conductance at long range appears more flat with respect to Δz than the green dotted line, being nearly length-independent. Such sharp conductance peaks at specific energy with a length-independent character is a hallmark of coherent resonant transport of noninteracting electrons.[14b,19] It is quite surprising that coherent resonant transport takes place in the twisted molecular wires. We reason as follows: a molecular wire is twisted when the tip-to-surface junction is narrow; when the junction is widened, the wire can have a straight section, which affords the resonant transport; when the junction is further widened, the twisted part retains its length while the straight section becomes longer. Experimentally, tip heights below 5 nm, the conductance decays exponentially. We believe that this is associated with the twisted wire conformation. At tip heights larger than 5 nm, nearly length-independent conductance is observed, which corresponds to wires containing a straight section.

We calculated the conductance of two strong contact junctions containing double and triple TPP units, as shown in Figure 4f. Here we focus on the negative bias region, where the LUMO level provides the conductance channels. Simulated dI/dV versus V traces are plotted in Figure 4f. The double-unit junction features a 31 nS conductance peak at −1.3 V (black trace), while the triple-unit junction features a 27 nS conductance peak at −1.6 V (red trace). The peak positions corroborate the shifting of the resonant conductance peak to more negative bias for the longer wire. The simulations reveal that the conductance peaks of both junctions are mediated by resonant transport via their LUMO levels (see the SI for details).

In conclusion, we have demonstrated that the conductance of single porphyrin oligomer wires exhibits nearly decayless differential conductance (β < 0.001 Å^{-1}) at long range (>6 nm). First-principles calculations revealed that the conductance is channeled by resonant transport through the delocalized LUMO. We anticipate that these findings will stimulate further efforts to use porphyrin oligomer wires to construct single-molecular electronics.

■ ASSOCIATED CONTENT

Supporting Information

The Supporting Information is available free of charge on the ACS Publications website at DOI: 10.1021/jacs.6b07416.

DOI: 10.1021/jacs.6b07416
J. Am. Chem. Soc. 2016, 138, 11140−11143

Methods and details of simulations of various junctions (PDF)

AUTHOR INFORMATION

Corresponding Authors

*phnlin@ust.hk

*liupn@ecust.edu.cn

Notes

The authors declare no competing financial interest.

ACKNOWLEDGMENTS

This work was supported by the Hong Kong RGC (16301415, N_HKUST601/15) and the National Natural Science Foundation of China (Projects 11274105, 21421004, 21561162003, and 21190033).

REFERENCES

(1) (a) Tao, N. J. *Nat. Nanotechnol.* **2006**, *1*, 173. (b) Marquardt, C. W.; Grunder, S.; Blaszczyk, A.; Dehm, S.; Hennrich, F.; Lohneysen, H. v.; Mayor, M.; Krupke, R. *Nat. Nanotechnol.* **2010**, *5*, 863. (c) Metzger, R. M. *Chem. Rev.* **2015**, *115*, 5056. (d) Weiss, E. A.; Ahrens, M. J.; Sinks, L. E.; Gusev, A. V.; Ratner, M. A.; Wasielewski, M. R. *J. Am. Chem. Soc.* **2004**, *126*, 5577.

(2) (a) Weiss, E. A.; Wasielewski, M. R.; Ratner, M. A. *Top. Curr. Chem.* **2005**, *257*, 103. (b) Ferrer, J.; Garcia-Suarez, V. M. *J. Mater. Chem.* **2009**, *19*, 1696. (c) Nitzan, A. *Annu. Rev. Phys. Chem.* **2001**, *52*, 681. (d) Nitzan, A.; Ratner, M. A. *Science* **2003**, *300*, 1384. (e) Joachim, C.; Ratner, M. A. *Proc. Natl. Acad. Sci. U. S. A.* **2005**, *102*, 8801.

(3) (a) Giese, B.; Amaudrut, J.; Kohler, A. K.; Spormann, M.; Wessely, S. *Nature* **2001**, *412*, 318. (b) Berlin, Y. A.; Ratner, M. A. *Radiat. Phys. Chem.* **2005**, *74*, 124. (c) Choi, S. H.; Kim, B.; Frisbie, C. D. *Science* **2008**, *320*, 1482. (d) Khoo, K. H.; Chen, Y.; Li, S.; Quek, S. Y. *Phys. Chem. Chem. Phys.* **2015**, *17*, 77. (e) Yan, H.; Bergren, A. J.; McCreery, R.; Della Rocca, M. L.; Martin, P.; Lafarge, P.; Lacroix, J. C. *Proc. Natl. Acad. Sci. U. S. A.* **2013**, *110*, 5326. (f) Tuccitto, N.; Ferri, V.; Cavazzini, M.; Quici, S.; Zhavnerko, G.; Licciardello, A.; Rampi, M. A. *Nat. Mater.* **2009**, *8*, 41.

(4) (a) Reed, M. A.; Zhou, C.; Muller, C. J.; Burgin, T. P.; Tour, J. M. *Science* **1997**, *278*, 252. (b) Di Ventra, M.; Pantelides, S. T.; Lang, N. D. *Phys. Rev. Lett.* **2000**, *84*, 979. (c) Getty, S. A.; Engtrakul, C.; Wang, L.; Liu, R.; Ke, S. H.; Baranger, H. U.; Yang, W.; Fuhrer, M. S.; Sita, L. R. *Phys. Rev. B* **2005**, *71*, 241401.

(5) Ratner, M. A.; Davis, B.; Kemp, M.; Mujica, V.; Roitberg, A.; Yaliraki, S. *Ann. N. Y. Acad. Sci.* **1998**, *852*, 22.

(6) (a) Porath, D.; Bezryadin, A.; de Vries, S.; Dekker, C. *Nature* **2000**, *403*, 635. (b) Tans, S. J.; Devoret, M. H.; Dai, H. J.; Thess, A.; Smalley, R. E.; Geerligs, L. J.; Dekker, C. *Nature* **1997**, *386*, 474.

(7) Tanaka, T.; Osuka, A. *Chem. Soc. Rev.* **2015**, *44*, 943.

(8) (a) Sedghi, G.; Sawada, K.; Esdaile, L. J.; Hoffmann, M.; Anderson, H. L.; Bethell, D.; Haiss, W.; Higgins, S. J.; Nichols, R. J. *J. Am. Chem. Soc.* **2008**, *130*, 8582. (b) Sedghi, G.; Esdaile, L. J.; Anderson, H. L.; Martin, S.; Bethell, D.; Higgins, S. J.; Nichols, R. J. *Adv. Mater.* **2012**, *24*, 653. (c) Sedghi, G.; Garcia-Suarez, V. M.; Esdaile, L. J.; Anderson, H. L.; Lambert, C. J.; Martin, S.; Bethell, D.; Higgins, S. J.; Elliott, M.; Bennett, N.; Macdonald, J. E.; Nichols, R. J. *Nat. Nanotechnol.* **2011**, *6*, 517.

(9) Vail, S. A.; Krawczuk, P. J.; Guldi, D. M.; Palkar, A.; Echegoyen, L.; Tomé, J. P. C.; Fazio, M. A.; Schuster, D. I. *Chem. - Eur. J.* **2005**, *11*, 3375.

(10) Li, Z.; Park, T.-H.; Rawson, J.; Therien, M. J.; Borguet, E. *Nano Lett.* **2012**, *12*, 2722.

(11) (a) Susumu, K.; Frail, P. R.; Angiolillo, P. J.; Therien, M. J. *J. Am. Chem. Soc.* **2006**, *128*, 8380. (b) Kocherzhenko, A. A.; Patwardhan, S.; Grozema, F. C.; Anderson, H. L.; Siebbeles, L. D. A. *J. Am. Chem. Soc.* **2009**, *131*, 5522.

(12) (a) Grill, L.; Dyer, M.; Lafferentz, L.; Persson, M.; Peters, M. V.; Hecht, S. *Nat. Nanotechnol.* **2007**, *2*, 687. (b) Adisoejoso, J.; Lin, T.; Shang, X. S.; Shi, K. J.; Gupta, A.; Liu, P. N.; Lin, N. *Chem. - Eur. J.* **2014**, *20*, 4111.

(13) (a) Gottfried, J. M. *Surf. Sci. Rep.* **2015**, *70*, 259. (b) Wang, W.; Pang, R.; Kuang, G.; Shi, X.; Shang, X.; Liu, P. N.; Lin, N. *Phys. Rev. B* **2015**, *91*, 045440. (c) Mielke, J.; Hanke, F.; Peters, M. V.; Hecht, S.; Persson, M.; Grill, L. *J. Am. Chem. Soc.* **2015**, *137*, 1844.

(14) (a) Lafferentz, L.; Ample, F.; Yu, H.; Hecht, S.; Joachim, C.; Grill, L. *Science* **2009**, *323*, 1193. (b) Koch, M.; Ample, F.; Joachim, C.; Grill, L. *Nat. Nanotechnol.* **2012**, *7*, 713. (c) Nacci, C.; Ample, F.; Bleger, D.; Hecht, S.; Joachim, C.; Grill, L. *Nat. Commun.* **2015**, *6*, 7397.

(15) (a) Reecht, G.; Scheurer, F.; Speisser, V.; Dappe, Y. J.; Mathevet, F.; Schull, G. *Phys. Rev. Lett.* **2014**, *112*, 047403. (b) Chong, M. C.; Reecht, G.; Bulou, H.; Boeglin, A.; Scheurer, F.; Mathevet, F.; Schull, G. *Phys. Rev. Lett.* **2016**, *116*, 036802. (c) Reecht, G.; Bulou, H.; Scheurer, F.; Speisser, V.; Mathevet, F.; González, C.; Dappe, Y. J.; Schull, G. *J. Phys. Chem. Lett.* **2015**, *6*, 2987.

(16) Hihath, J.; Tao, N. *Prog. Surf. Sci.* **2012**, *87*, 189.

(17) Galperin, M.; Ratner, M. A.; Nitzan, A. *J. Phys.: Condens. Matter* **2007**, *19*, 103201.

(18) Liu, Z. F.; Wei, S. J.; Yoon, H.; Adak, O.; Ponce, I.; Jiang, Y.; Jang, W. D.; Campos, L. M.; Venkataraman, L.; Neaton, J. B. *Nano Lett.* **2014**, *14*, 5365.

(19) Datta, S. *Electronic Transport in Mesoscopic Systems*; Cambridge University Press: Cambridge, U.K., 1995.

DOI: 10.1021/jacs.6b07416
J. Am. Chem. Soc. 2016, 138, 11140−11143